THE JOURNAL OF PHYSICAL CHEMISTRY Letters

LETTER

pubs.acs.org/JPCL

Raman Scattering and Electronic Heating in Molecular Conduction Junctions

Michael Galperin*,† and Abraham Nitzan*,‡

†Department of Chemistry & Biochemistry, University of California at San Diego, La Jolla, CA 92093, USA

‡School of Chemistry, Tel Aviv University, Tel Aviv, 69978, Israel

ABSTRACT: Surface-enhanced Raman scattering (SERS) was recently used to monitor nonequilibrium properties of molecular conduction junctions. Ward et al. (Nat. Nanotechnol. 2011, 6, 33) have used such measurements to estimate heating of the molecular vibrations (indicated by the ratio between Stokes and anti-Stokes Raman peaks) as well as the electronic metal substrate (inferred from the corresponding components of the Raman continuum). The latter observation suggests, contrary to standard assumptions, significant heating of the metal contacts. Here, we discuss this observation by advancing a theory of the electronic Raman scattering background in biased current carrying molecular junctions and using it to estimate the electronic heating, as seen in the Raman signal. We reach the unexpected conclusion that while heating of the electronic background in Raman scattering from biased molecular junctions is indeed observed, this does not necessarily imply an appreciable deviation from thermal equilibrium in the electronic distributions in the leads.

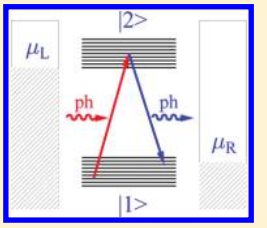

SECTION: Electron Transport, Optical and Electronic Devices, Hard Matter

Studies of Raman scattering from molecular conduction junctions lie at the juncture of two contemporary fields of research, molecular electronics and molecular plasmonics. Typical configurations of such junctions are similar to structures discussed as "hot spots" in SERS studies of single molecules.[1,2] Indeed, this enhancement was important for getting detectable signals in recent studies of Raman scattering from such junctions.[3−5] Observed correlation between junction conductivity and its Raman scattering signal[4] indicate that Raman scattering can probe structural changes in the junction that affect its conductivity.

The issue of heating in biased molecular junctions has attracted considerable experimental[3,5−10] and theoretical[11−13] attention, motivated by the relevance of this phenomenon to current induced chemical change and junction stability.[14,15] Such studies rely on finding a suitable probe. Raman scattering provides such a probe[3,5] that can, in principle, be applied separately to different modes by monitoring the ratio between the Stokes and anti-Stokes components of the scattering signal.[16] It is a common practice to describe such heating by an effective temperature, although this concept is ill-defined in nonequilibrium situations. Ward and co-workers[5] were able not only to assign effective temperatures to molecular vibrations but also to observe heating of the underlying electronic continuum. This continuum is usually attributed to electronic excitations in the metal substrate(s), and the latter result significantly suggests that heating of the metal contacts cannot be ignored, in contrast to usual practice. Junction heating can be caused by direct interaction with the incident light.[5] Here, we focus on the additional heating resulting from the current through the molecular bridge in a biased junction. As explained below, this heating is confined to the neighborhood of the molecule−metal contact, and its manifestation in the electronic Raman spectrum must result from the molecular contribution to this spectrum. To focus on this effect, we assume that both conduction and light−matter interaction are mediated by the molecule and disregard direct charge transfer between the metal electrodes and direct light−metal interaction. We invoke the model used in our previous publications[17,18] (see Figure 1 of ref 17), a two-level (HOMO−LUMO) molecule coupled to two metal contacts L and R, represented by free electron reservoirs characterized by electrochemical potentials μ_L and μ_R, respectively. The Hamiltonian is

$$\hat{H} = \sum_{m=1,2} \varepsilon_m \hat{d}_m^\dagger \hat{d}_m + \sum_{k \in \{L,R\}} \varepsilon_k \hat{c}_k^\dagger \hat{c}_k + \sum_{m=1,2} \sum_{k \in \{L,R\}} (V_{km} \hat{c}_k^\dagger \hat{d}_m + \text{H.c.}) + \sum_\alpha (\hbar \nu_\alpha \hat{a}_\alpha^\dagger \hat{a}_\alpha + U_\alpha \hat{a}_\alpha \hat{d}_2^\dagger \hat{d}_1 + \text{H.c.}) \quad (1)$$

and the metal−molecule coupling is characterized by the functions $\Gamma_m^K(E) \equiv 2\pi \Sigma_{k \in K} |V_{km}|^2 \delta(E - \varepsilon_k)$ and $\Gamma_m \equiv \Sigma_{K=L,R} \Gamma_m^K$ (K = L,R). Here, $\hat{d}_m^\dagger$ ($\hat{d}_m$) and $\hat{c}_k^\dagger$ ($\hat{c}_k$) are creation (annihilation) operators of an electron in state m on the molecule and state k in the contact, respectively. The last term in eq 1 describes the radiation field and its interaction with the molecule, where $\hat{a}_\alpha^\dagger$ ($\hat{a}_\alpha$) are creation (annihilation) operators of photons in optical mode α. In a possible scenario for the observed electronic heating, the electronic current creates a region in the metal, near the metal−molecule contact, where the electronic distribution is out of equilibrium. Because of the fast (10−100 fs) relaxation of electrons in metals, this region is very small; however Raman

Received: June 30, 2011
Accepted: August 3, 2011

scattering, dominated by the molecule−radiation field interaction and affected by the molecule−metal interaction, probes exactly this nonequilibrium region.

Consider first the electronic distributions in the leads. An upper limit on its deviation from equilibrium is obtained by assuming that in the contact regions that contribute to the inelastic light scattering signal through their interaction with the molecule thermal relaxation can be disregarded, so that this distribution is dominated by the transmission process. Accordingly, in terms of the junction transmission function $T(E)$, the nonequilibrium electronic distributions in the leads are given by

$$\begin{aligned} f_{\mathrm{K}}^{\mathrm{SS}}(E) &= \frac{1}{2}[f_{\mathrm{K}}(E) + (1 - T(E))f_{\mathrm{K}}(E) + T(E)f_{\bar{\mathrm{K}}}(E)] \\ &= f_{\mathrm{K}}(E) + \frac{1}{2}T(E)[f_{\bar{\mathrm{K}}}(E) - f_{\mathrm{K}}(E)] \end{aligned} \tag{2}$$

where K = L(R), $\bar{\mathrm{K}}$ = R(L), and $f_{\mathrm{K}}(E) = [\mathrm{e}^{(E-\mu_{\mathrm{K}})/k_{\mathrm{B}}T} + 1]^{-1}$ (where k_{B} is the Boltzmann constant and T is the temperature). In the calculations reported below, we use the result for nonoverlapping resonances, $T(E) = \Sigma_{m=1,2}(\Gamma_m^{\mathrm{L}}\Gamma_m^{\mathrm{R}})/[(E - \varepsilon_m)^2 + (\Gamma_m/2)^2]$. Using eq 2, an effective temperature for each electrode may be defined by requiring zero heat flux between the nonequilibrium steady-state distribution $f_{\mathrm{K}}^{\mathrm{SS}}(E)$ and an equilibrium thermal bath with the same chemical potential μ_{K} and effective temperature T_{eff}

$$\int \frac{\mathrm{d}E}{2\pi}(E - \mu_{\mathrm{K}})[f_{\mathrm{K}}^{\mathrm{SS}}(E) - f_{\mathrm{K}}(E, T_{\mathrm{eff}})] = 0 \tag{3}$$

Next consider the light scattering process. We focus only on inelastic light scattering associated with energy imparted to electronic excitations in the leads and therefore omit molecular vibrations from our consideration. The electronic inelastic spectrum accompanies the Raleigh scattering in the calculation discussed below and will similarly dress vibrationally inelastic signals in a full model calculation.

Our calculation follows the procedure described in our earlier publications.[16,18] It leads to the steady-state scattering flux from an incident photon mode of frequency ν_{i} to the outgoing frequency ν_{f}

$$\begin{aligned} J_{\nu_i \to \nu_f} &= \frac{2\pi}{\hbar}|U_i|^2|U_f|^2\rho(\nu_i)\rho(\nu_f)\{\delta(\hbar\nu_i - \hbar\nu_f) \\ &\left|\int \frac{dE^{(1)}}{2\pi}\int \frac{dE^{(2)}}{2\pi}\frac{G_2^{>}(E^{(2)})G_1^{<}(E^{(1)})}{\hbar\nu_i + E^{(1)} - E^{(2)} + i\delta}\right|^2 \end{aligned} \tag{4a}$$

$$\begin{aligned} &+ \int \frac{dE_i^{(1)}}{2\pi}\int \frac{dE_f^{(1)}}{2\pi}\delta(\hbar\nu_i + E_i^{(1)} - \hbar\nu_f - E_f^{(1)}) \\ &G_1^{<}(E_i^{(1)})G_1^{>}(E_f^{(1)})\left|\int \frac{dE^{(2)}}{2\pi}\frac{G_2^{>}(E^{(2)})}{\hbar\nu_i + E_i^{(1)} - E^{(2)} + i\delta}\right|^2 \end{aligned} \tag{4b}$$

$$\begin{aligned} &+ \int \frac{dE_i^{(2)}}{2\pi}\int \frac{dE_f^{(2)}}{2\pi}\delta(\hbar\nu_i + E_i^{(2)} - \hbar\nu_f - E_f^{(2)}) \\ &G_1^{<}(E_i^{(2)})G_2^{>}(E_f^{(2)})\left|\int \frac{dE^{(1)}}{2\pi}\frac{G_1^{<}(E^{(1)})}{\hbar\nu_i + E^{(1)} - E_f^{(2)} + i\delta}\right|^2 \end{aligned} \tag{4c}$$

$$\begin{aligned} &+ \int \frac{dE_i^{(1)}}{2\pi}\int \frac{dE_f^{(1)}}{2\pi}\int \frac{dE_i^{(2)}}{2\pi}\int \frac{dE_f^{(2)}}{2\pi} \\ &\delta(\hbar\nu_i + E_i^{(1)} + E_i^{(2)} - \hbar\nu_f - E_f^{(1)} - E_f^{(2)}) \\ &\left\{\frac{G_1^{<}(E_i^{(1)})G_1^{>}(E_f^{(1)})G_2^{<}(E_i^{(2)})G_2^{>}(E_f^{(2)})}{\left|\hbar\nu_i + E_i^{(1)} - E_f^{(2)} + i\delta\right|^2}\right\} \end{aligned} \tag{4d}$$

where $\rho(\nu_{\mathrm{f}})$ ($\sim\nu^3$ in free space) is the density of final photon states and $G_m^{>,<}(E)$ (m = 1,2) are single-particle Green functions

$$G_m^{>}(E) = -\mathrm{i}\sum_{\mathrm{K=L,R}}\frac{\Gamma_m^{\mathrm{K}}[1 - f_{\mathrm{K}}(E)]}{(E - \varepsilon_m)^2 + (\Gamma_m/2)^2} \tag{5}$$

$$G_m^{<}(E) = \mathrm{i}\sum_{\mathrm{K=L,R}}\frac{\Gamma_m^{\mathrm{K}}f_{\mathrm{K}}(E)}{(E - \varepsilon_m)^2 + (\Gamma_m/2)^2} \tag{6}$$

Within the model as described, $\delta \to 0+$. More generally, δ should be replaced by broadening of the optical signal due to interaction with the environment. In the calculations discussed below, the Fermi functions in eqs 5 and 6 can be taken to be the equilibrium Fermi distributions in the leads, as is usually done in junction transport calculations, or the distribution given by eq 2 that reflects the maximum possible heating of the corresponding leads. (To use the distribution eq 2 in the transport calculation, one needs to assume that momentum relaxation is fast while energy relaxation is slow on the relevant time scale. Indeed, the momentum relaxation time for metallic electrons is $\sim 10^{-14}$ s,[19] 1−2 orders of magnitude faster than the corresponding energy relaxation.[20]) Below, we compare results obtained from these two choices.

The term eq 4a clearly corresponds to Rayleigh scattering. Equations 4b and 4c account for inelastic scattering where the change in electronic occupation of metal states occurs near the lower and the upper molecular levels, respectively. Equation 4d describes an inelastic scattering process that involves change of states of two electrons. Because only metal states that are energetically close to molecular states make an appreciable contribution to these fluxes and because change in an electronic state requires a partially filled level, light scattering will be enhanced whenever a lead Fermi energy is close to a molecular level. This observation underlines much of the dependence of the scattering flux on the bias voltage that is reported below. From this flux, we can calculate the Raman temperature using the Stokes/anti-Stokes ratio according to

$$T_{\mathrm{Raman}} = \frac{\Delta\nu}{\ln\left(\frac{J_{\nu_i \to \nu_i - \Delta\nu}}{J_{\nu_i \to \nu_i + \Delta\nu}} \times \frac{\rho(\nu_i + \Delta\nu)}{\rho(\nu_i - \Delta\nu)}\right)} \tag{7}$$

(We use the free space relationship $\rho(\nu) \approx \nu^3$. This may be modified in the junction cavity, which adds a measure of uncertainty in the experimental determination of T_{Raman}.)

Equilibrium results ($\mu_{\mathrm{L}} = \mu_{\mathrm{R}}$) are shown in Figure 1. Equation 4c dominates here because (for our choice of parameters) level 2 is closer to the Fermi energy and consequently characterized by more pronounced partial population, while the population of level 1 is nearly 1. We see (inset) that at equilibrium, the Raman estimate accurately follows the actual junction temperature. Furthermore, the Raman estimate does not depend on the Raman shift used (see the dotted line in Figure 2a).

dx.doi.org/10.1021/jz2008853 |J. Phys. Chem. Lett. 2011, 2, 2110–2113

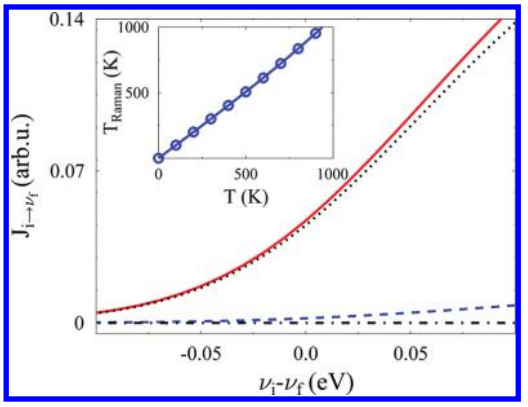

Figure 1. Equilibrium calculation. The electronic Raman intensity $J_{i\to\nu_f}$ as function of the Raman shift $\Delta\nu = \nu_i - \nu_f$ at $T = 300$ K. The solid (red) line shows the overall light scattering intensity, while the other lines correspond to the different contributions, eq 4b (dashed, blue), eq 4c (dotted, black) and eq 4d (dashed−dotted, black). (Inset) The electronic Raman temperature obtained from the Stokes/anti-Stokes ratio (eq 7) plotted against the equilibrium contacts temperature ($|\Delta\nu| = |\nu_i - \nu_f| = 0.05$ eV was used in this calculation, but the result does not depend on this particular choice as long as $|\Delta\nu|$ is not too large). Junction parameters are $\Gamma^L_m = \Gamma^R_m = 0.25$ eV, $m = 1, 2$, $\mu_L = \mu_R = 0$, $\varepsilon_1 = -1.5$ eV, $\varepsilon_2 = 1$ eV. The incoming photon frequency is $\nu_i = 2$ eV.

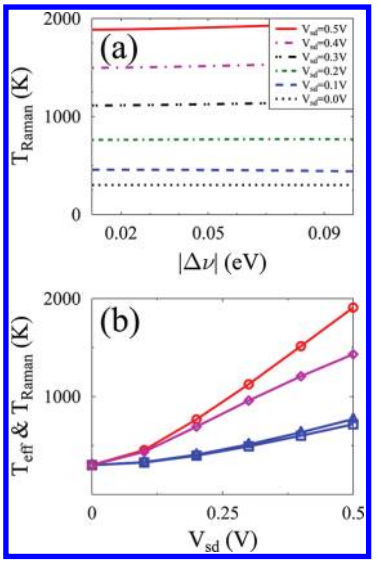

Figure 2. Low bias results, $|e|V_{sd} = \mu_L - \mu_R \ll \varepsilon_2 - \varepsilon_1$. (a) The electronic Raman temperature (eq 7) plotted against the inelastic shift for different voltage biases. (b) A comparison between the Raman temperature (circles, red) (eq 7) and the effective electronic temperatures of contacts L (triangles, blue) and R (squares, blue) obtained from eq 3 and the effective molecular temperature (eq 8) (diamonds, magenta) displayed against the voltage bias. The bias is applied symmetrically, that is, $\mu_L = |e|V_{sd}/2$ and $\mu_R = -|e|V_{sd}/2$. Other parameters are as those in Figure 1. Results obtained by using the equilibrium thermal distributions in the leads are almost indistinguishable from those obtained using the nonequilibrium distribution of eq 2.

Figure 2 shows low bias results. The Raman temperature remains independent of the Raman shift for small shifts (Figure 2a) and is compared to the effective electronic temperatures of the two leads, obtained from eq 3 (Figure 2b). We see that while both estimates indicate heating, the calculated

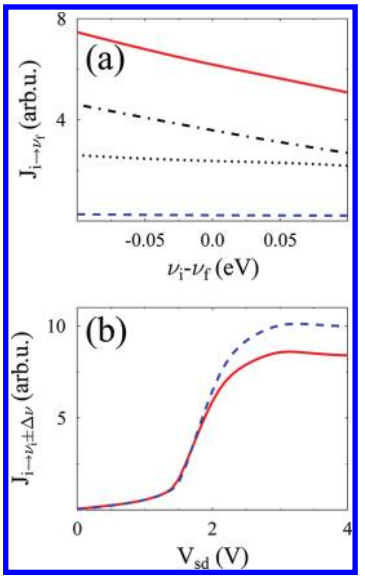

Figure 3. Nonequilibrium calculation at high bias. (a) The electronic Raman intensity $J_{i\to\nu_f}$ displayed against the Raman shift $\Delta\nu = \nu_i - \nu_f$ for $V_{sd} = 2$ V. The solid (red) line shows the overall light scattering intensity, while the other lines correspond to the different contributions, eq 4b (dashed, blue), eq 4c (dotted, black) and eq 4d (dashed−dotted, black). (b) Stokes (solid line, red) and anti-Stokes (dashed line, blue) intensities for $\Delta\nu = 0.025$ eV versus the voltage bias. Other parameters are as those in Figure 1.

temperatures are considerably different. Another important observation (not shown) is that the Raman temperature evaluated from eqs 4−7 almost does not depend on whether we use eq 2 or the equilibrium Fermi functions for the junctions' electronic disributions. This indicates that T_{Raman} reflects the bias potential mostly through the nonequilibrium electronic distribution in the molecule and is only weakly sensitive to the relatively small distortion of the metal electronic distribution.

To further confirm this conclusion, we introduce yet another temperature estimate, the effective molecular electronic temperature, T_M. It is obtained by assigning an electronic chemical potential, μ_M, to the molecule as described below and then defining T_M from

$$\int \frac{dE}{2\pi}(E-\mu_M)\sum_{m=1,2}\left(f(E,\mu_M,T_M)G^{>}_m(E) + [1-f(E,\mu_M,T_M)]G^{<}_m(E)\right) = 0 \quad (8)$$

which has a requirement, analogous to eq 3, that the heat current between the molecule and a fictitious equilibrium free electron bath, characterized by the same chemical potential μ_M and the effective temperature T_M, vanish.[12] For the effective molecular chemical potential μ_M, we take an estimate based on extending the equilibrium expression $\mu = (\partial E/\partial n)$ to steady state, $\mu_M = (dE/dt)/(dn/dt) = J_E/J_e$, where J_E and J_e are energy and electron currents through the molecule.[12] The effective molecular electronic temperature T_M obtained in this way is shown by the magenta (diamond) line in Figure 2b. We see that the Raman temperature is in much better agreement with T_M than with the effective temperatures of the leads.

When the bias increases (Figure 3), the electrochemical potentials of the leads come close to the molecular levels, and all of the terms in eqs 4b and 4c can be important. For high

dx.doi.org/10.1021/jz2008853 |J. Phys. Chem. Lett. 2011, 2, 2110–2113

enough bias, eq 4d, which requires partially populated metal electronic states near both levels 1 and 2, can dominate the inelastic electronic spectrum (compare Figures 1a and 3a). Densities of electron and hole states contributing to this process may lead to situations where the anti-Stokes signal exceeds the Stokes intensity, making the Raman temperature meaningless.

The SERS background may result from direct light−metal interation and from interaction mediated by the molecule. Here, we focused on the second contribution that dominates the current-induced heating in the metal leads. (The dominating effect of the molecules can be seen by comparing I/V and heating signals in Figure 4a,d of ref 5.) We have advanced a theory for the Raman background in a biased current carrying molecular junctions and have shown that this signal indeed carries heating information; however rather than reflecting the state of the metal contacts as implied by ref 5, the observed heating is dominated by the electronic nonequilibrium in the molecular bridge and can be at least qualitatively reproduced without invoking electrode heating.

The fact that the different temperature estimates discussed are different is a significant although not very surprising observation for a nonequilibrium junction. At high bias, while heating is clearly observed, the Raman temperature becomes meaningless as the anti-Stokes intensity may exceed the Stokes signal.

■ ACKNOWLEDGMENT

We acknowledge support by the Israel Science Foundation (A.N.), the Israel−US Binational Science Foundation (A.N. and M.G.), the European Science Council (A.N., FP7/ERC Grant No. 226628), the Israel−Niedersachsen Research Fund (A.N.), and the NSF (M.G., CHE-1057930). We thank Doug Natelson for sharing his data prior to publication and for valuable comments and Mark Ratner for many helpful discussions.

■ REFERENCES

(1) Nie, S.; Emory, S. R. Probing Single Molecules and Single Nanoparticles by Surface-Enhanced Raman Scattering. *Science* **1997**, *275*, 1102–1106.

(2) Michaels, A. M.; Jiang, J.; Brus, L. Ag Nanocrystal Junctions as the Site for Surface-Enhanced Raman Scattering of Single Rhodamine 6G Molecules. *J. Phys. Chem. B* **2000**, *104*, 11965–11971.

(3) Ioffe, Z.; Shamai, T.; Ophir, A.; Noy, G.; Yutsis, I.; Kfir, K.; Cheshnovsky, O.; Selzer, Y. Detection of Heating in Current-Carrying Molecular Junctions by Raman Scattering. *Nat. Nanotechnol.* **2008**, *3*, 727–732.

(4) Ward, D. R.; Halas, N. J.; Ciszek, J. W.; Tour, J. M.; Wu, Y.; Nordlander, P.; Natelson, D. Simultaneous Measurements of Electronic Conduction and Raman Response in Molecular Junctions. *Nano Lett.* **2008**, *8*, 919–924.

(5) Ward, D. R.; Corley, D. A.; Tour, J. M.; Natelson, D. Vibrational and Electronic Heating in Nanoscale Junctions. *Nat. Nanotechnol.* **2011**, *6*, 33–38.

(6) Agrait, N.; Untiedt, C.; Rubio-Bollinger, G.; Vieira, S. Onset of Energy Dissipation in Ballistic Atomic Wires. *Phys. Rev. Lett.* **2002**, *88*, 216803.

(7) Huang, Z.; Xu, B.; Chen, Y.; Di Ventra, M.; Tao, N. Measurement of Current-Induced Local Heating in a Single Molecule Junction. *Nano Lett.* **2006**, *6*, 1240–1244.

(8) Tsutsui, M.; Taniguchi, M.; Kawai, T. Local Heating in Metal−Molecule−Metal Junctions. *Nano Lett.* **2008**, *8*, 3293–3297.

(9) Tsutsui, M.; Taniguchi, M.; Kawai, T. Single-Molecule Identification via Electric Current Noise. *Nat. Commun.* **2010**, *1*, 138.

(10) Steiner, M.; Freitag, M.; Perebeinos, V.; Tsang, J. C.; Small, J. P.; Kinoshita, M.; Yuan, D.; Liu, J.; Avouris, P. Phonon Populations and Electrical Power Dissipation in Carbon Nanotube Transistors. *Nat. Nanotechnol.* **2009**, *4*, 320–324.

(11) Galperin, M.; Ratner, M. A.; Nitzan, A. Molecular Transport Junctions: Vibrational Effects. *J. Phys.: Condens. Matter* **2007**, *19*, 103201.

(12) Galperin, M.; Nitzan, A.; Ratner, M. A. Heat Conduction in Molecular Transport Junctions. *Phys. Rev. B* **2007**, *75*, 155312.

(13) Pecchia, A.; Romano, G.; Di Carlo, A. Theory of Heat Dissipation in Molecular Electronics. *Phys. Rev. B* **2007**, *75*, 035401.

(14) Lorente, N.; Rurali, R.; Tang, H. Single-Molecule Manipulation and Chemistry with the STM. *J. Phys.: Condens. Matter* **2005**, *17*, S1049.

(15) Jorn, R.; Seideman, T. Implications and Applications of Current-Induced Dynamics in Molecular Junctions. *Acc. Chem. Res.* **2010**, *43*, 1186–1194.

(16) Galperin, M.; Ratner, M. A.; Nitzan, A. Raman Scattering from Nonequilibrium Molecular Conduction Junctions. *Nano Lett.* **2009**, *9*, 758–762.

(17) Galperin, M.; Nitzan, A. Optical Properties of Current Carrying Molecular Wires. *J. Chem. Phys.* **2006**, *124*, 234709.

(18) Galperin, M.; Ratner, M. A.; Nitzan, A. Raman Scattering in Current-Carrying Molecular Junctions. *J. Chem. Phys.* **2009**, *130*, 144109.

(19) Güdde, J.; Rohleder, M.; Meier, T.; Koch, S. W.; Höfer, U. Time-Resolved Investigation of Coherently Controlled Electric Currents at a Metal Surface. *Science* **2007**, *318*, 1287–1291.

(20) Arbouet, A.; Voisin, C.; Christofilos, D.; Langot, P.; Del Fatti, N.; Vallee, F.; Lerme, J.; Celep, G.; Cottancin, E.; Gaudry, M.; et al. Electron−Phonon Scattering in Metal Clusters. *Phys. Rev. Lett.* **2003**, *90*, 177401.